Modification of Ti6Al4V Substrates with Well-defined Zwitterionic Polysulfobetaine Brushes for Improved Surface Mineralization

Pingsheng Liu, Emily Domingue, David C. Ayers, and Jie Song*

Department of Orthopedics & Physical Rehabilitation, Department of Cell & Developmental Biology, University of Massachusetts Medical School, Worcester, Massachusetts 01655, United States

S *Supporting Information*

ABSTRACT: Osteoconductive mineral coatings are beneficial for improving the osteointegration of metallic orthopedic/dental implants, but achieving adequate structural integration between the surface minerals and underlying metallic substrates has been a significant challenge. Here, we report covalent grafting of zwitterionic poly(sulfobetaine methacrylate) (pSBMA) brushes on the Ti6Al4V substrates to promote the surface-mineralization of hydroxyapatite with enhanced surface mineral coverage and mineral-substrate interfacial adhesion. We first optimized the atom transfer radical polymerization (ATRP) conditions for

synthesizing pSBMA polymers in solution. Well-controlled pSBMA polymers (relative molecular weight up to 26kD, PDI = 1.17) with high conversions were obtained when the ATRP was carried out in trifluoroethanol/ionic liquid system at 60 °C. Applying identical polymerization conditions, surface-initiated atom transfer radical polymerization (SI-ATRP) was carried out to graft zwitterionic pSBMA brushes (PDI < 1.20) from the Ti6Al4V substrates, generating a stable superhydrophilic and low-fouling surface coating without compromising the bulk mechanic property of the Ti6Al4V substrates. The zwitterionic pSBMA surface brushes, capable of attracting both cationic and anionic precursor ions during calcium phosphate apatite mineralization, increased the surface mineral coverage from 32% to 71%, and significantly reinforced the attachment of the apatite crystals on the Ti6Al4V substrate. This facile approach to surface modification of metallic substrates can be exploited to generate multifunctional polymer coatings and improve the performance of metallic implants in skeletal tissue engineering and orthopedic and dental care.

KEYWORDS: Ti6Al4V, surface modification, zwitterionic brush, SI-ATRP, calcium phosphate apatite, mineralization
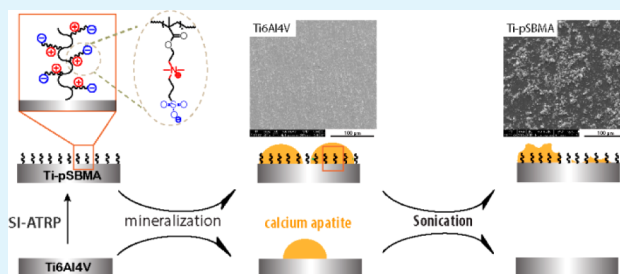
INTRODUCTION

Titanium and its alloys are extensively used in orthopedics and dentistry as implants because of their excellent mechanical properties and corrosion resistance.[1−3] The stable surface oxide layer (up to 10 nm in thickness) spontaneously formed when exposed in air confers biocompatibility.[4] However, lack of adequate osteointegration of the metallic implant with surrounding skeletal tissues could lead to early implant failure, which remains one of the most significant challenges in its clinical applications.[5] Numerous attempts have been made to address this challenge, including generating porous implant surfaces[6,7] or increasing surface roughness[8−10] to facilitate bone in-growth, introducing osteoconductive bioceramic coatings (e.g., hydroxyapatite, HA) to promote bone cell attachment,[11,12] and locally delivering osteogenic growth factors (e.g., rhBMP-2) on implant surfaces to stimulate its osteointegration.[13,14] Among these approaches, the introduction of bioactive minerals to implant surfaces is particularly attractive, as it could simultaneously confer osteoconductivity to improve cellular attachment, drug delivery capability, and long-term biocompatibility due to the bone mineral-like compositions.[14−16] The apatite mineral component could also absorb and retain endogenously secreted protein factors from the *in vivo* bony tissue environment,[17] further promoting *in vivo*

osteointegration. Plasma spray of calcium apatite and *in vitro* heterogeneous mineralization employing various mineralization conditions[15,18−20] have been utilized to create surface mineral coatings to metallic implants. The plasma spray technique has tremendous advantage in terms of its facile control of the thickness of the ceramic coating applied to the implant and is thus the primary commercial choice. The heterogeneous mineralization approach, if templated by proper mineral nucleation sites presented on the metallic implant surfaces, could be beneficial to not only the preimplantation generation of osteoconductive coating but also *in vivo* osteointegration during the dynamic implant surface remodeling postimplantation. Major barrier for translating the latter strategy into commercial and clinical uses, however, is the inadequate adherence of the surface minerals to the metallic substrate due to suboptimal choice/presentation of surface mineral nucleation sites (e.g., often the surface oxides are utilized for templating the mineralization).[15] The identification of potent mediators of heterogeneous mineralization and their robust

presentation on the metallic implant surface with controlled surface densities are highly desired, yet not adequately explored.

In natural biomineralization, both negatively and positively charged residues in the collagen fibrils have been shown to play pivotal roles in recruiting precursor ions, lowering interfacial energy for heterogeneous nucleation, stabilizing amorphous calcium phosphate (ACP), and mediating the subsequent transformation from ACP into oriented apatite crystals.[21−24] Emulating nature's strategy, we recently demonstrated that synthetic zwitterionic sulfobetaine hydrogels, possessing oppositely charged residues to attract both precursor cations and anions, could effectively template extensive heterogeneous HA-mineralization throughout the three-dimensional (3-D) scaffold with excellent structural integration.[25] In addition, zwitterionic materials, well-known for their low-fouling nature and biocompatibility,[26−29] have been widely explored for applications as blood compatible materials[30,31] and DNA and protein delivery vehicles.[32,33] Taken together, these properties have led us to hypothesize that zwitterionic polymer coatings, when applied to titanium substrates with good bonding affinity (e.g., via covalent grafting), could promote the heterogeneous nucleation and growth of calcium apatite minerals on the implant surface with improved interfacial affinity, thereby potentially improving the implant osteointegration *in vivo*.

Surface-initiated atom transfer radical polymerization (SI-ATRP) is a well-established method for grafting uniform functional polymer brushes from various substrates.[34] By covalently tethering initiators to the surface of interest, ATRP of vinyl monomers could be triggered from the surface to generate well-controlled functional polymer brushes via the living radical polymerization.[35−37] Silane coupling agents have long been used for tethering to titanium substrates.[35,37−41] The Ti−O−Si bond formed, however, exhibits quite low hydrolytic stability.[42] In contrast, phosphonic acid-terminated small molecules have been shown to form stable Ti−O−P bonds on titanium surfaces with better surface coverage and improved hydrolytic stability under physiological conditions compared to silanes[40,42,43] and was previously utilized to successfully form self-assembled monolayers on the metallic surface.[43] In this study, we developed robust chemistry and optimal SI-ATRP conditions to covalently tether phosphonic acid−based initiators onto Ti6Al4V substrates and graft well-controlled zwitterionic poly(sulfobetaine methacrylate) (pSBMA) brushes from the Ti6Al4V substrates. The surface properties of the pSBMA-grafted substrates were characterized by XPS analyses, contact angle measurements, and nonspecific protein absorptions. The improvement in *in vitro* mineralization templated by Ti6Al4V with *vs* without grafted pSBMA surface brushes, in terms of both the extent of the surface mineral coverage and their affinity to the metallic substrate, was characterized.

■ EXPERIMENTAL SECTION

Materials. [2-(Methacryloyloxy)ethyl]dimethyl-(3-sulfopropyl)-ammonium hydroxide (SBMA, 97%), ethyl α-bromoisobutyrate (EBiB, 98%), α-bromoisobutyryl bromide (BiBB, 98%), 2,2′-bipyridyl (BPY, 97%), copper(I) bromide (CuBr, 99.999%), 1-hexyl-3-methylimidazolium chloride (HMImCl, 97%), 2,2,2-trifluoroethanol (TFE, 99%), bromotrimethylsilane (BTMS, 97%), anhydrous methanol (99.8%), anhydrous dichloromethane (DCM, 99.8%), anhydrous hexane (95%), and acetone (99.9%) were purchased from Sigma-Aldrich and used as received. Triethylamine (TEA, 99.5%, Sigma-Aldrich) was dried by calcium hydride (CaH₂, 99.99%, Sigma-Aldrich) and distilled prior to use. Diethyl (hydroxymethyl)-phosphonate (P−OH, 98%, TCI America) was used as received.

Bovine serum albumin (BSA)-fluorescein conjugate was purchased from Invitrogen and used as received. Ti6Al4V plate (1.3 mm thick, Titanium Metal Supply Inc.) was cut into 10 × 10 mm² square pieces or 4 × 40 mm² strips, which were sequentially polished under water with 600, 1500, and 3000 grit silicon carbide sandpapers and ultrasonically cleaned with hexane (10 min), DCM (10 min), and acetone (10 min) sequentially. After the extensive washing, the substrates were annealed in a 120 °C oven prior to use. The porous region of a commercial Ti6Al4V hip stem (Taperloc, Complete Hip Stem, BioMet) was cut into 10 × 10 × 10 mm³ cubic pieces, and treated in the same manner as described for the Ti6Al4V plates except that no polishing was carried out with the porous stem surface.

General Instrumentation. ^{1}H NMR (400 MHz), ^{13}C NMR (100 MHz), and ^{31}P NMR (170 MHz) spectra were recorded in methanol-d₄ on a Varian INOVA-400 spectrometer. The proton and carbon signals of TMS were used as internal reference for ^{1}H NMR and ^{13}C NMR, while phosphoric acid was added for calibration of the ^{31}P NMR. Mass spectra were acquired on a Thermo LTQ in a positive ion mode. The samples were dissolved in water (1 mg/mL) and diluted in 50% MeOH to 10 μg/mL and infused using a Triversa Nanomate into the Thermo LTQ.

Synthesis of (Diethoxyphosphoryl)methyl 2-Bromo-2-methylpropanoate (P−O−Br). P−OH (1.68 g, 10 mmol) and TEA (1.52 g, 15 mmol) were mixed in 20 mL of anhydrous DCM in a dry, two-neck flask equipped with a dropping funnel and sealed with rubber stoppers. The mixture was cooled in an ice bath before 20 mL of DCM solution of BiBB (3.45 g, 15 mmol) was slowly added via the dropping funnel. The esterification reaction (synthetic scheme shown in Supporting Information (SI) Figure S1) proceeded in the ice bath for 1 h and then continued at room temperature for 24 h. After being washed with 10% HCl aqueous solution (4 times, 45 mL each time), the organic phase was dried with anhydrous calcium sulfate and concentrated under reduced pressure yielding a brown oil-like crude product. The product was purified by flash chromatography with ethyl acetate as an eluent to obtain clear oil product (63.6% yield). ^{1}H NMR (400 MHz, methanol-d₄): δ 4.46 (d, J = 8.5 Hz, 2H), 4.18 (m, 4H), 1.94 (s, 6H), δ 1.34 (t, J = 7.1 Hz, 6H) ppm; ^{13}C NMR (100 MHz, methanol-d₄): δ 170.7, 63.4, 63.4, 58.3, 56.6, 54.9, 29.9, 15.6, 15.6 ppm; ^{31}P NMR (170 MHz, methanol-d₄): δ 17.8 ppm. MS (ESI, m/z) for C₉H₁₈Br₁O₅P₁: [M + H]⁺ calculated, 317.09, found 317.11.

Synthesis of Initiator (2-Bromo-2-methylpropanoyloxy) Methylphosphonic Acid (PA−O−Br). The deprotection of P−O−Br was carried out in a two-step process (synthetic scheme shown in SI Figure S1). P−O−Br (1.06 g, 3.34 mmol) was dissolved in 20 mL of anhydrous DCM in a dry flask, to which BTMS (1.86 g, 12 mmol) was subsequently added by injection. The reaction proceeded at room temperature under argon atmosphere overnight before volatile components and DCM were removed under vacuum. Anhydrous methanol (15 mL) was then added to the intermediate and stirred at room temperature overnight before the solvent and volatiles were removed under vacuum yielding a yellowish oil. After recrystallization in DCM, the product was obtained as white crystals (47% yield). ^{1}H NMR (400 MHz, methanol-d₄): δ 4.39 (dd, J = 9.0, 1.6 Hz, 2H), 1.94 (s, 6H) ppm. ^{13}C NMR (100 MHz, methanol-d₄): δ 171.1, 60.1, 58.5, 55.2, 29.9 ppm. ^{31}P NMR (170 MHz, methanol-d₄): δ 14.9 ppm. MS (ESI, m/z) for C₅H₁₀Br₁O₅P₁: [M + H]⁺ calculated, 261.01, found 261.09. All original NMR and MS spectra are shown in SI Figures S2−S5.

Surface Immobilization of Initiator PA−O−Br on Ti6Al4V. Annealed Ti6Al4V substrates (40 pieces) were cleaned in an air plasma cleaner (Harrick, PDC-001) for 2 min before being placed in a plastic dish, and submerged under 40 mL of 3-mM anhydrous methanol solution of PA−O−Br at room temperature in dark for 24 h to allow the phosphonic acid group to attach to the thin oxidized metallic surface. All retrieved substrates (Ti−Br) were then annealed at 110 °C for 15 min in a vacuum oven, followed by extensive sonication in methanol (10 min each time, twice), and dried under vacuum.

Optimization of the Conditions for ATRP of Zwitterionic SBMA. To optimize the ATRP conditions, a series of polymerizations

Table 1. ATRP of SBMA in TFE or HMImCl/TFE (10 wt %) Solutions

run	DP	solvent	temp. (°C)	reaction time (h)	conversion (%)[a]	M_n (theo) (g/mol)	M_n (GPC) (g/mol)	PDI
1	100	TFE	23	19	>99	27 851	19 382	1.26
2	100	HMImCl/TFE	23	21	93	26 175	15 321	1.14
3	50	HMImCl/TFE	60	18.5	99	14 023	12 643	1.13
4	100	HMImCl/TFE	60	6	90	25 337	16 823	1.14
5	200	HMImCl/TFE	60	21.5	93	52 154	25 478	1.17

[a]Determined by ^{1}H NMR.

varying the reaction temperature and with/without the introduction of HMImCl (1:10 by weight relative to TFE used[44]) were carried out (Table 1). In a typical procedure, BPY (0.2 mmol) was dissolved in TFE in a Schlenk flask and degassed by three "freeze-pump-thaw" cycles to remove oxygen. The flask was then backfilled with argon and CuBr (0.1 mmol) was added into the flask under the argon protection. The mixture was stirred for 10 min to ensure the formation of the copper catalyst complex. Monomer SBMA (10 mmol, for DP = 100), free initiator EBiB (0.1 mmol), and HMImCl were dissolved in TFE under stirring in the second Schlenk flask at room temperature. The flask was then degassed by three "freeze−pump−thaw" cycles, after which the copper catalyst complex was added by syringe. The mixture was allowed to stir for an additional 1 min before the flask was mounted in an isothermal water bath to start the polymerization. During the course of the reaction, aliquots of the reaction mixture were retrieved at various time points for ^{1}H NMR and GPC monitoring of the ATRP reaction. After the predetermined time, the reactor was exposed to air to terminate the polymerization and the resulting mixture was precipitated in methanol to obtain free zwitterionic pSBMA polymer.

Grafting pSBMA Polymer Brushes from Ti−Br Surfaces by SI-ATRP. The SI-ATRP was conducted under the optimized conditions (with the introduction of HMImCl and under 60 °C). The process was similar to that of the solution ATRP described above. Instead of conducting the polymerization in the second Schlenk flask, the mixture was quickly transferred into a flat-bottom reactor containing Ti−Br substrates under argon atmosphere after the 1 min's stirring, ensuring the SI-ATRP and solution ATRP were almost simultaneously progressed. When the polymerization was completed, the pSBMA-grafted Ti6Al4V substrates (e.g., Ti-pSBMA-100, where 100 refers to the targeting degree of polymerization, DP) were extracted with TFE using a Soxhlet apparatus for 24 h to remove the free polymer physically absorbed on the surface and dried under vacuum. pSBMA brushes with different targeting DPs (50, 200) were grafted from Ti−Br by varying the ratio of monomers relative to initiators accordingly.

Torsion Test. To evaluate the bulk mechanical property of the Ti substrates before and after modification, torsion tests of Ti6Al4V and Ti-pSBMA substrates ($1.3 \times 4 \times 40$ mm^3 stripes, $n = 3$) were performed on an MTS Bionix 370 test system equipped with a 150 kN/150 N-m load cell from 0 to 70° at 0.2°/s at room temperature. Torsional stiffness of the substrates was calculated from the linear region (0 to 15°) of the respective torque-displacement curves.

Cleavage of pSBMA Brushes from the pSBMA-Grafted (Ti-pSBMA) Substrates. The Ti-pSBMA substrates were placed in a 50 mL plastic Corning tube containing 30 mL of ionic acidic cleaving solution (0.2 M NaCl and 2 M HCl aqueous solution) and subjected to gentle shaking on an orbital shaker at room temperature for 72 h. The cleavage solution was then collected, neutralized by sodium hydroxide, and desalted in a dialysis membrane tubing (Spectra/Por 6, MWCO: 1000) against Milli-Q water for 72 h, with regular change of fresh Milli-Q water every 8 h. Cleaved pSBMA was obtained after freeze-drying for subsequent analyses.

Aqueous Gel Permeation Chromatography (GPC). GPC of solution polymers or those cleaved from the substrates were performed on a Varian ProStar HPLC system connected with two PL Aquagel−OH columns (type 40 first, followed by type 20, 8 mm, 300 × 7.5 mm, Agilent Technologies) and equipped with a refractive index detector (Varian 356-LC, 35 °C). The eluent was 0.05 M Trisma

buffer (pH 7.0) containing 0.2 M NaNO$_3$ and a flow rate of 1.0 mL/min was applied. Weight- and number-averaged molecular weights (M_w and M_n) and polydispersity index (PDI) of the polymers were calculated by Cirrus AIA GPC software. Ten narrowly dispersed PEO standards from PL2070-0100 and PL-2080-0101 kits (Polymer Laboratories, Agilent Technologies) were used as calibration standards.

X-ray Photoelectron Spectroscopy (XPS). Surface compositional analyses of substrates before and after SI-ATRP were carried out on a Thermo Scientific K-Alpha XPS equipped with an Al K$_\alpha$ radiation source under the pass energy of 200 or 50 eV (for survey or high resolution scan) and the spot size of 400 μm. Survey scan spectra were obtained from five consecutive scans of a randomly chosen area of interest while high resolution scan spectra were obtained from ten consecutive scans. All binding energies were referenced to the C$_{1s}$ hydrocarbon peak at 285.0 eV.

Water Contract Angle Measurements. The static water contact angles of the substrates before and after surface modifications were recorded on a CAM200 goniometer (KSV Instruments). A droplet (2 μL) of Milli-Q water was placed on the substrate and the contact angles (left and right) of the droplet were recorded after 30 s. The left and right contact angles of each droplet, and three substrates of each sample group were averaged and reported as averages ± standard deviation.

Nonspecific Protein Adsorption on Surfaces. Ti6Al4V substrates with or without grafted pSBMA were placed in a 24-wells culture plate containing 1 mL of BSA-fluorescein conjugate/DPBS solution (500 μg/mL) in each well and incubated at 37 °C overnight. All substrates were rinsed with fresh DPBS (pH 7.4) three times upon retrieval to move loosely absorbed BSA. The substrate surfaces were then imaged on a Zeiss inverted stage fluorescent microscope. The fluorescence intensities were quantified by ImageJ using line plots.

Surface Mineralization. Mineralization was carried out by controlled heating of the Ti6Al4V substrates with or without grafted pSBMA in a urea-containing, acidic solution of hydroxyapatite from 37 to 95 °C using a protocol modified over a previous report,[45] which has been identified as a more efficient heterogeneous mineralization process than the SBF method.[15] Mineralization stock solution was prepared by suspending hydroxyapatite (7.37 g, 34−40% Calcium content, Alfa Aesar) in 500 mL aqueous solution of urea (2 M), followed by the addition of concentrated hydrochloric acid under constant stirring until a clear soluble solution was obtained (final pH 2.5−3.0). Six to ten Ti substrates were placed in an Erlenmeyer flask containing 30 mL of the mineralization solution and covered with a perforated aluminum foil. The flask was placed in a high-temperature silicone oil bath with the mineralization solution completely submerged under the oil and heated by a 100-W immersion heater (Glo-Quartz LHP-IAH4) equipped with a programmable temperature controller (Eurotherm 2408). Controlled heating from 37.0 to 95.0 °C was carried out at a heating rate of 0.2 °C/min. Mineralized substrates were bath-sonicated for 1 min in Milli-Q water to ensure the removal of loosely bound mineral precipitates and dried under vacuum before further use or characterizations.

Quantification of Surface Calcium Content. Total calcium content of the mineralized substrates was determined by quantifying the Ca^{2+} ions released ($n = 3$) from the substrate upon treatment in a hydrochloric acid solution with a Thermo Scientific calcium ion selective electrode attached to a VWR Symphony pH/ISE meter. In a typical procedure, the mineralized substrate was placed in 10 mL of

hydrochloric acid solution (pH 3) in a 20 mL glass vial and the pH was adjusted by concentrated hydrochloric acid to around 2.1. The mineral was allowed to be fully released from the substrate under constant shaking of the acidic solution on an orbital shaker. Ionic Strength Adjustment buffer (ISA, 4 M KCl solution, VWR, 200 μL) was added to the acidic solution containing the released calcium prior to measurement by the calcium ion selective electrode. The total calcium content of each type of mineralized substrate was determined using a standard curve generated by a series of acidic (pH 2.1) aqueous Ca^{2+} ion standard solutions containing 0.1, 0.01, 0.001, and 0.0001 M $CaCl_2$.

Scanning Electron Microscopy (SEM) and Associated Energy Dispersive X-ray Spectroscopy (EDS). The morphology of the dried mineralized substrate, coated with 3 nm carbon, was observed on a Quanta 200 FEG MKII scanning electron microscope (SEM, FEI) under an accelerating voltage of 5 or 10 kV, with a spot size of 3.0 μm (aperture 6) and a working distance about 10 mm. EDS was acquired under 10 kV, with a spot size of 3.0 μm. Reported calcium to phosphorus ratios (Ca/P) were calibrated against single crystal HA whiskers prepared by molten salt synthesis (Ca/P = 1.67).[46]

Cell Viability and Proliferation Assay. To evaluate the cytocompatibility of the surface coatings (pSBMA brushes and the surface mineralization), the viability of rat bone marrow-derived stromal cells (rMSCs) cultured in the presence of Ti6Al4V, Ti-pSBMA, and the mineralized Ti-pSBMA substrates were tested by CCK-8 cell proliferation kit (Dojindo). The Ti6Al4V, Ti-pSBMA, and mineralized Ti-pSBMA substrates (n = 3) were sterilized in ethanol (15 min immersion) and air-dried in a ventilated tissue culture hood. The substrates pre-equilibrated in sterile PBS (pH 7.4) and cell culture medium (α-MEM with 20% FBS, 1% penicillin, and 1% streptomycin, 2% glutamine) were transferred into 24-well culture plate containing 1 mL of fresh medium in each well, to which rMSC (passage 1) suspension (10 μL, 20 000 cells) was added and cultured for up to 72 h. Comparing to directing seeding of cells on metallic surfaces only, this chosen method of cell seeding ensures comparable overall number of adherent cells in each well regardless of the nature of the metallic surfaces (e.g., pSBMA-grafted surfaces are known for reduced cell adhesiveness), thereby ensuring fair comparison of substrate cytocompatibility. Comparing to the other alternative of placing metallic substrates over an established adherent MSC culture, this method also ensures that the access to nutrients and the proliferation of cells are not impeded. At 24 or 72 h after initial cell seeding, cell culture medium in each well was replaced with 0.4 mL of fresh medium along with 40 μL CCK-8 reagents and incubated for 4 h. The absorbance of the removed culture media was read at 450 nm (background subtraction at 620 nm) on a microplate reader.

■ RESULTS AND DISCUSSION

Optimization of ATRP of SBMA in TFE Solution. Unlike that of conventional polar vinyl monomers, the ATRP of zwitterionic sulfobetaine monomer tend to be poorly controlled in conventional polar solvents (including water) because the strong electrostatic interactions between the oppositely charged residues of the sulfobetaine monomers and polymers[47] compromise their solubility, resulting in polymers with a broad molecular weight distributions (MWD).[48] Recently, homogeneous polymerization of sulfobetaine monomers was reported in fluoroalchohol/ionic liquid systems. The well-controlled polymerization mediated by ionic liquid HMImCl and the improved polymer solubility in TFE yielded high molecular weight (MW) polysulfobetaines (up to 305 kDa in MW) with narrow MWD (PDI ~ 1.20).[44] Thus, the TFE and TFE/HMImCl systems were investigated to identify optimal conditions for mediating well-controlled ATRP of SBMA in the current study.

The ATRP of SBMA in TFE only was first carried out at room temperature with CuBr and BPY as the catalyst and
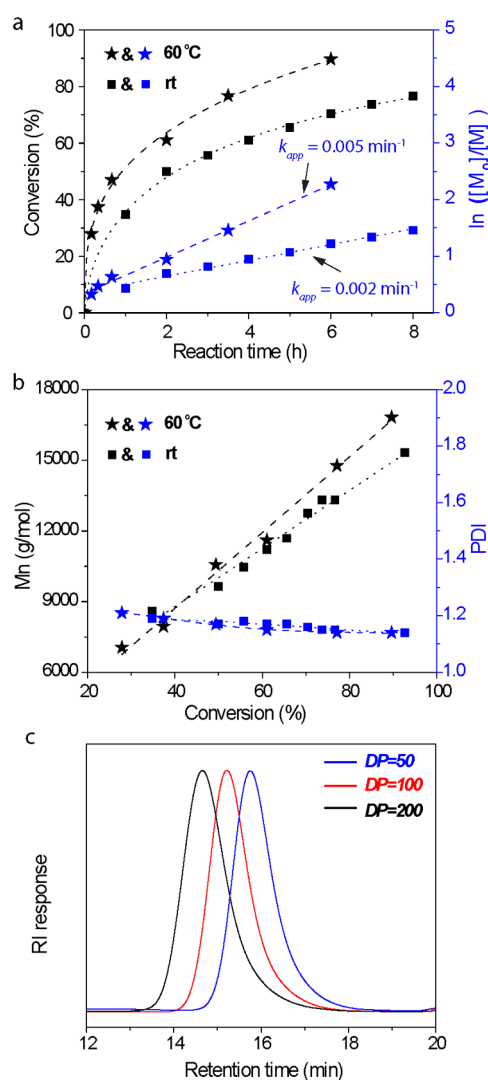
Figure 1. Well-controlled ATRP of zwitterionic SBMA carried out in 10 wt % HMImCl in TFE. (a) Monomer conversion (%) and conversion index $\ln([M]/[M]_0)$ as a function of reaction time at room temperature (rt) (squares) and 60 °C (stars). (b) Molecular weight and polydispersity index (PDI) as a function of monomer conversion (%) at rt (squares) and 60 °C (stars). [SBMA] = 1 M, [SBMA]/[EBiB]/[CuBr]/[BPY] = 100:1:1:2. (c) GPC traces of pSBMA with different degree of polymerizations (DPs) prepared in 10 wt % HMImCl/TFE at 60 °C (PDI and Mn summarized in Table1).

catalyst ligand, respectively (Table 1, run 1). Over 80% of the monomers were converted into polymers within the first hour in a pseudo-first-order reaction kinetics, with an apparent propagation rate constant (k_{app}) of 0.011 min^{-1} (SI Figure S6), supporting that the highly polar TFE enabled rapid monomer conversions. The MWD (M_n =19 382, PDI = 1.26) of the resulting pSBMA was narrower than those obtained in a water/methanol system (with PDI rapidly increasing from 1.26 to 1.47 when M_n increased from 4764 to 90 340) where the electrostatic aggregation of pSBMA in the poor nonionic solvent had likely compromised the exposure of the reactive ends for continued propagation.[48]

The ATRP of SBMA in TFE was significantly slowed with the introduction of ionic liquid imidazolium chloride (HMImCl, 10 wt % relative to TFE; Table 1, run 2). Only 35% of the SBMA monomers were converted after 1 h and 93%

7144

dx.doi.org/10.1021/am501967y | ACS Appl. Mater. Interfaces 2014, 6, 7141–7152
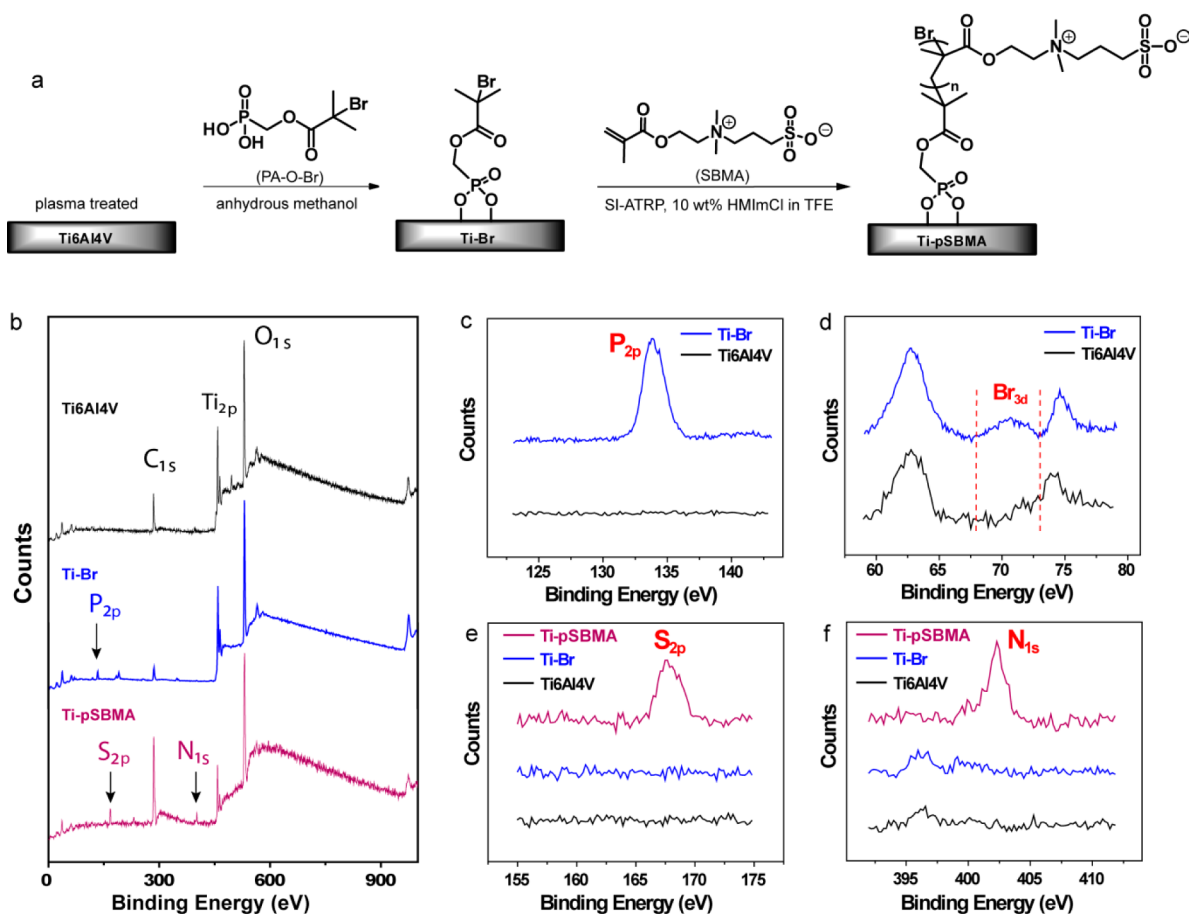
Figure 2. Grafting of pSBMA brushes from the Ti6Al4V substrate. (a) Schematic illustration of the grafting of pSBMA brushes from the Ti6Al4V substrate by SI-ATRP. (b) XPS survey scans on the Ti6Al4V surfaces before and after immobilization of anchorable initiators and subsequent SI-ATRP. (c) High resolution scans of P_{2p} of Ti6Al4V and Ti—Br surfaces. (d) High resolution scans of Br_{3d} of the Ti6Al4V and Ti—Br surfaces; the binding energy range of Br_{3d} is indicated by the red dash lines. (e) High resolution scans of S_{2p} of Ti6Al4V, Ti—Br, and Ti-pSBMA surfaces. (f) High resolution scans of N_{1s} of Ti6Al4V, Ti—Br, and Ti-pSBMA surfaces.

converted after 21 h in the present of HMImCl as revealed by ^{1}H NMR monitoring (Figure 1a, black squares). The k_{app} decreased to one-fifth of that in TFE alone (0.002 min^{-1} vs 0.011 min^{-1}, Figure 1a blue squares). However, the resulting pSBMA polymers with relative molecular weights up to 15 321 (Figure 1b, black squares) remained narrowly dispersed (PDI = 1.14, Figure 1b, blue squares, SI Figure S7a), suggesting that the polymerization proceeded without significant side reactions, active chain end termination, or deactivation in the presence of the ionic liquid. Combined with the first-order kinetics revealed by linear plot of $\ln(M_0/M)$ vs reaction time and the linear increase of MW over time (Figure 1b, black squares), these data support HMImCl as a promising mediator for controlled ATRP of sulfobetaine. Similar trend was previously observed with the ATRP of other electrolyte monomer.[49] The mechanism of how ionic liquid affects the ATRP of electrolyte monomers has not been fully revealed. Takahara et al. proposed that the ionic liquid may have shifted the equilibrium between the active species (radical) and the dormant species (C—Br), by electron-donating to the Cu^{II} complex thereby facilitating the deactivation of the active species, toward the dormant species side.[43] Such a scenario could have led to slower polymerization with suppressed chain termination.

Further optimization of the reaction was carried out in TFE/HMImCl by elevating temperature while keeping other parameters unchanged (Table 1, run 4). We showed that, at 60 °C, 50% of the monomers (vs 35% at room temperature) were converted in 1 h at an accelerated rate (k_{app} of 0.005 min^{-1}, Figure 1a, star symbols). Despite the increased reaction kinetics, the ATRP remained well-controlled in the presence of the ionic liquid at 60 °C as characterized by the first-order kinetics (linear plot of $\ln(M_0/M)$ vs reaction time, Figure 1a, blue stars) and the linear increasing of the MW with narrow MWDs over time (PDI = 1.14 for M_n = 16,823, Figure 1b, star symbols; SI Figure S7b). Using the optimized polymerization medium of 10 wt % HMImCl in TFE and the elevated temperature of 60 °C, well-controlled pSBMA polymers (PDI ≤ 1.17, relative MW up to 25,478) with targeted degrees of polymerizations (DPs) of 50, 100, and 200 were prepared (Table 1, run 3−5; Figure 1c). This optimized solvent and temperature were then extended to the subsequent SI-ATRP for grafting pSBMA brushes from Ti6Al4V substrates.

Grafting pSBMA Brushes from Ti6Al4V Substrates by SI-ATRP. To create stably anchored SI-ATRP initiator on the Ti6Al4V surface, phosphonic acid-terminated initiator PA—O—Br, synthesized in three steps (SI Figure S1), was used to form stable Ti—O—P bonds. Air plasma-cleaned Ti6Al4V substrates were soaked in 3 mM of PA—O—Br/methanol solution for 24 h and then annealed at 110 °C to immobilize PA—O—Br on the surface (Figure 2a). The successful surface immobilization of the PA—O—Br on Ti6Al4V was confirmed by the detection of the characteristic XPS signals for P_{2p} (binding energy of 133.9
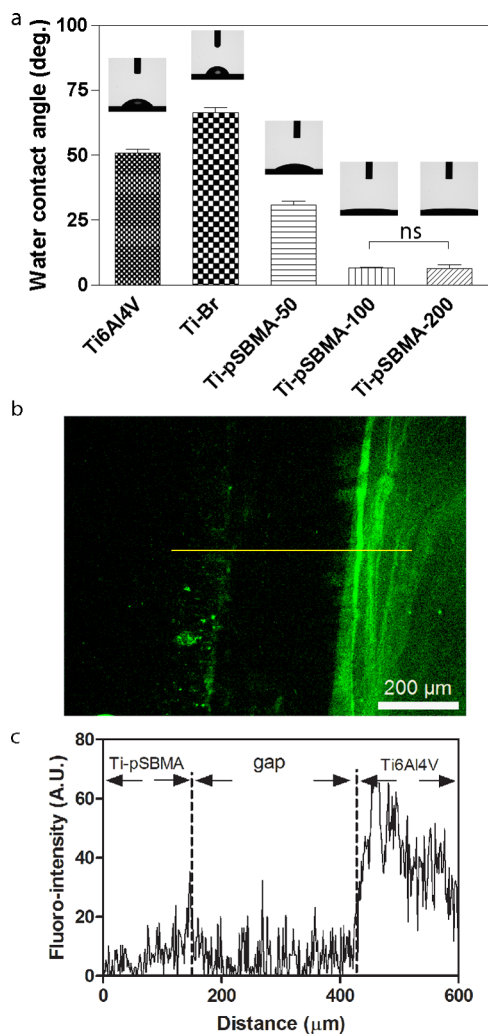
Figure 3. (a) Water contact angles on Ti6Al4V, Ti−Br, and the Ti-pSBMA surfaces with different DPs of grafted pSBMA brushes ($n = 3$). All differences are significant ($P < 0.05$, one-way ANOVA multiple comparison) unless denoted as ns (not significant). (b) Fluorescent micrograph, and (c) Fluorescent intensity line plot showing substantially reduced nonspecific absorption of fluorescein-conjugated BSA on the Ti6Al4V substrate upon surface grafting of pSBMA (DP = 200).

eV) and Br_{3d} (70.5 eV) core electrons that were absent from the unmodified Ti6Al4V surface (Figure 2b−d). Of note, the bromine signal detected on the Ti−Br surface was weaker than that of the phosphorus signal (0.37% of Br vs 6.39% of P) and did not match their 1:1 stoichiometric ratio in PA−O−Br. Although the high-temperature annealing process enhanced the bonding of PA−O−Br to the Ti6Al4V substrate (e.g., only 0.18% of Br and 4.27% of P was detected by XPS from the Ti−Br substrate without annealing), it could have also potentially destabilized the terminal bromine residue. Meanwhile, it has also been reported that the C−Br bond was unstable under X-ray irradiation during XPS analysis,[50] leading to similar observations.[51]

Grafting pSBMA brushes from the Ti−Br substrate via SI-ATRP was carried out in the optimized TFE/HMImCl system at 60 °C in the presence of EBiB as the sacrificial free initiator. After extensive extraction of the modified substrates with TFE to move physically absorbed free polymers, the surface composition of the resulting Ti-pSBMA substrate was characterized by XPS. Two characteristic peaks corresponding to the core electrons of S_{2p} (167.5 eV) and N_{1s} (402.5 eV) and originating from the zwitterionic sulfobetaine side chains, were detected from the survey scans of Ti-pSBMA but not the Ti−Br substrates (Figure 2b). The S and N signal intensities (4.02% of S vs 4.62% of N) revealed by the high-resolution scans (Figure 2e and f) approximated their 1:1 stoichiometric ratio, which, along with the significantly decreased Ti signals resulting from surface polymer coverage, supported successful grafting of the pSBMA brushes from the Ti6Al4V substrate.

The grafting of superhydrophilic zwitterionic pSBMA brushes also resulted in the expected changes in surface wettability of the Ti6Al4V substrate by water. As showed in Figure 3a, the immobilization of the Br-terminated initiator resulted in an increase in surface hydrophobicity (increase of the water contact angle from 50° to 62°) whereas subsequent grafting of pSBMA brushes with a DP of 50 sharply reduced the water contact angle by half. When pSBMA brushes with higher DP of 100 were grafted, the hydrophilicity of the surface that were more densely covered by the zwitterionic polymer brushes further increased, resulting in an exceptionally low water contact angel of ∼10°. However, increasing DP of the grafted pSBMA from 100 to 200 did not further decrease the surface water contact angles.

Finally, we verified the successful grafting of pSBMA by examining the antibiofouling property of the surface modified with the zwitterionic polymer.[52−55] As shown in Figure 3b, whereas significant nonspecific absorption of fluorescein-labeled BSA on Ti6Al4V substrates was observed upon incubation of the substrate in the protein solution followed by copious rinsing, almost no absorption was detected from the substrate grafted with pSBMA brushes (Ti-pSBMA-200), which was further validated by the quantitative line plot analysis of the detected fluorescent intensities of both substrate surfaces (Figure 3c). These data suggest that the grafted pSBMA brushes sufficiently covered the Ti6Al4V surface and conferred the antifouling property characteristic of the zwitterionic polymer.

Impact of Grafting pSBMA by SI-ATRP on the Surface Morphology and Mechanical Properties of Ti6Al4V and the Stability of the Surface Brushes. We investigated whether/how grafting pSBMA brushes by SI-ATRP changes the surface morphology or compromises the mechanical property of the Ti6Al4V substrates. Low magnification (1000×) SEM micrographs revealed similar polishing trails of the substrates with and without grafting of pSBMA brushes while the higher magnification (25 000×) SEM micrographs confirmed that grafting pSBMA by SI-ATRP did not induce significant changes in surface morphologies of the substrates on the micrometer scale (Figure 4a). Torsional mechanical properties of the substrates remained largely unaffected upon grafting pSBMA as supported by the overlapping torque-displacement curves of Ti6Al4V and Ti-pSBMA substrates (Figure 4b). No statistically significant difference in torsional stiffness of the substrates was detected (Figure 4c). These observations support that the SI-ATRP process did not compromise the mechanical integrity of the Ti6Al4V substrates.

To investigate the stability of the grafted pSBMA brushes, the Ti-pSBMA substrates were subjected to bath-sonication in TFE for 30 min (note that all substrates were extracted in TFE, a good solvent for free pSBMA, for 24 h to remove physically absorbed free polymers prior to sonication). The retrieved substrates were then rinsed with fresh TFE, vacuum-dried, and
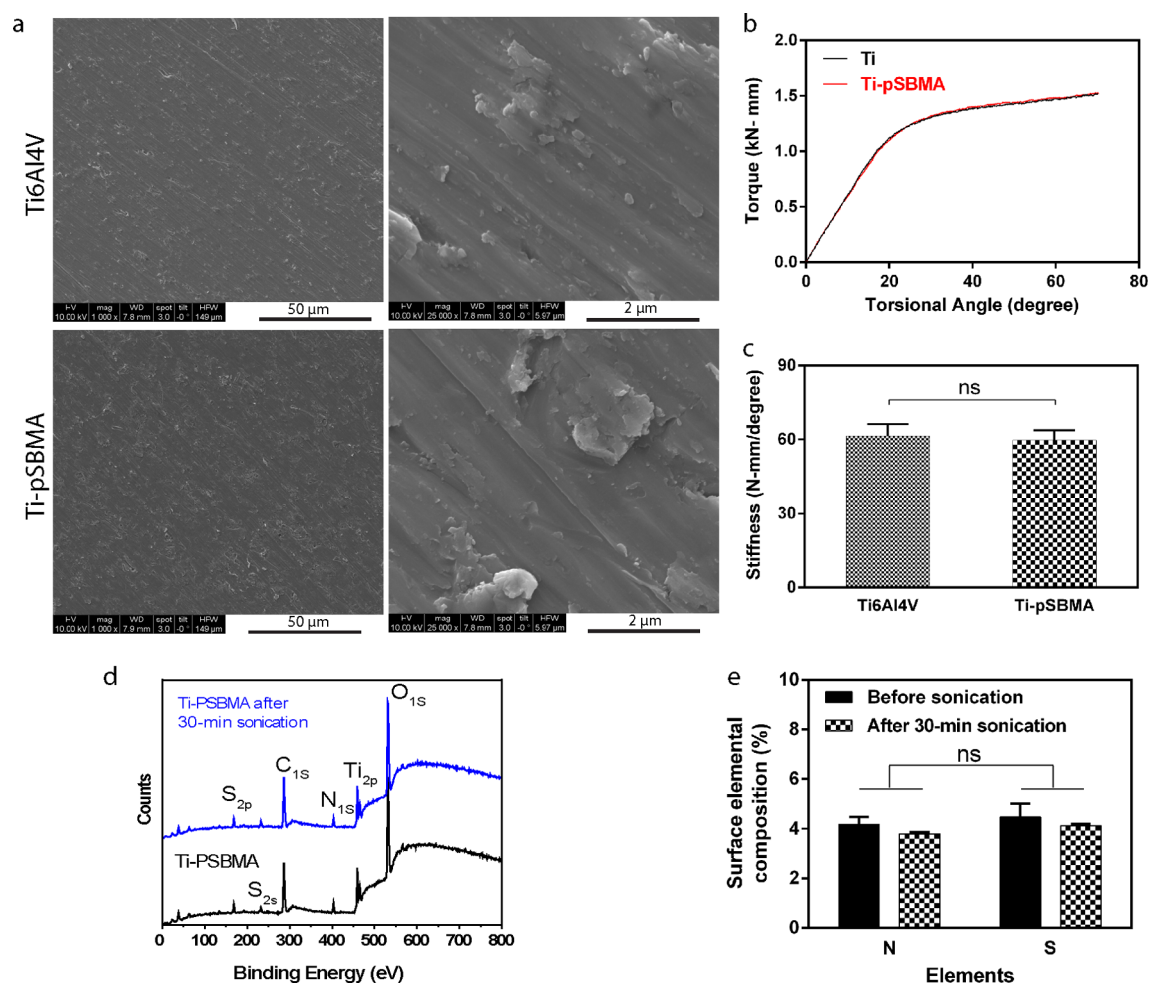
Figure 4. Surface morphology and mechanical property of the Ti6Al4V substrates before and after grafting pSBMA brushes and the stability of the pSBMA brush coating. (a) SEM micrographs of Ti6Al4V and Ti-pSBMA surfaces. (b) Torque-displacement curves of of Ti6Al4V and Ti-pSBMA substrates. (c) Torsional stiffness of Ti6Al4V and Ti-pSBMA substrates ($n = 3$). The difference was not significant ($P > 0.05$, Student's t test). (d) XPS survey scans of the Ti-pSBMA surfaces before and after 30 min ultrasonication in TFE. (e) N and S elemental contents (determined by XPS high resolution scans of N_{1s} and S_{2p}) on the Ti-pSBMA substrates ($n = 3$) before and after 30 min ultrasonication in TFE. No significant differences detected ($P > 0.05$, two-way ANOVA multiple comparison).

Table 2. Properties of the Solution pSBMA vs Surface-Grafted pSBMA Cleaved from the Ti-pSBMA Substrate

| no.	polymer type	M_n (theo) (g/mol)	M_n (GPC) (g/mol)	PDI
a[a]	free	38 187	19 710	1.18
b[b]	free	38 187	19 576	1.18
c[c]	brush		17 246	1.15

[a]Free polymer (initiated by with the sacrificial free initiators in solution). [b]Free polymer of a, but treated with the acidic cleavage solution (2-M HCl, 72 h). [c]Brush polymer cleaved by 2-M HCL (72 h) from the Ti-pSBMA substrate prepared in the same pot of SI-ATRP as those in a.

subjected to XPS analysis. From the survey scans (Figure 4d), the N and S signals associated with the pSBMA brushes were observed with similar intensities with and without the sonication of Ti-pSBMA. Furthermore, quantitation of the N and S elemental contents by high-resolution scans (Figure 4e) confirmed that not only the absolute contents but also the stoichiometric ratio of these elements remained the same after the sonication treatment, supporting that the pSBMA brushes were stably grafted to the Ti6Al4V substrate.

Characterization of the Surface-Grafted pSBMA Brushes. To characterize the MW and MWD of the grafted pSBMA brushes on the Ti6Al4V surface, the Ti-pSBMA substrates were incubated in 2-M HCl aqueous solution. The cleaved polymer solution was neutralized with NaOH, desalted by dialysis and freeze-dried for GPC analyses. As shown in Table 2, the grafted pSBMA brushes exhibited a narrow MWD (PDI = 1.15, M_n = 17 246) similar to that of the free polymers formed with the sacrificial free initiator in the solution (PDI = 1.18, M_n = 19 710) from the same pot polymerization, supporting that a well-controlled SI-ATRP of SBMA was accomplished.

To examine whether the relatively lower MW of the grafted pSBMA compared to that of the free pSBMA (by 13%, Table 2, Figure 5a) was due to the hydrolysis of the zwitterionic side chains during the acidic cleavage, we subjected the free pSBMA to the same acid treatment. GPC and 1H NMR analyses of the free pSBMA before and after the acid treatment revealed no difference in the polymer retention time, MW, PDI (Figure 5a, entries a and b in Table 2) or the proton integration ratio between the backbone methyl group ($C–CH_3$) and the side chain methyl group ($N–CH_3$) (Figure 5b). Thus, we conclude
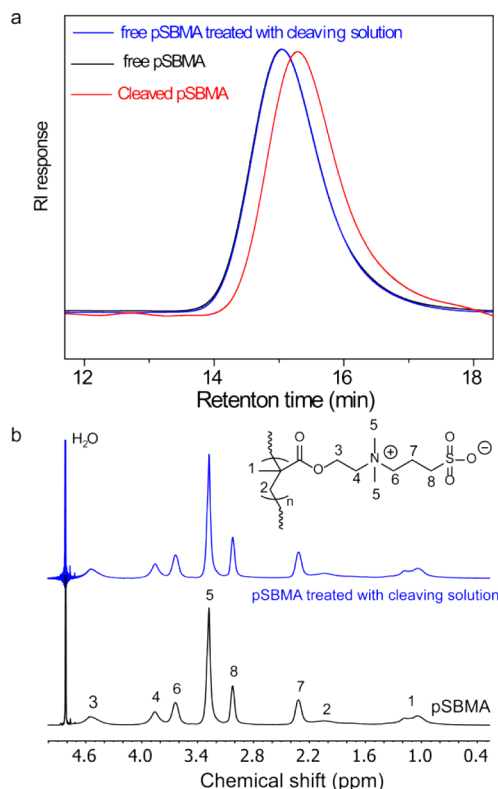
Figure 5. (a) GPC traces of pSBMA cleaved from Ti-pSBMA (red) and the free pSBMA formed in solution before (black) and after acid treatment (blue). (b) ¹H NMR spectra of the free pSBMA formed in solution before (black) and after acid treatment (blue).

that the side chains of the pSBMA remained stable during the grafted brush cleaving process, and the lower MW observed with the grafted pSBMA was likely a result of the relatively slower kinetics of the SI-ATRP compared to that of the solution ATRP taking place in the same pot. The surface-bound initiator presented on Ti−Br substrate as well as the propargating reactive chain ends[56,57] of the polymers grafted from the substrate have intrinsically reduced degrees of freedom compared to the free initiators and free propagating polymers in the solution, thus fewer chances to encounter monomers and consequently relatively slower propagation rate and lower MW obtainable in a given time. Indeed, although the addition of free initiators into the SI-ATRP system is a widely accepted method to determine the DP of solution polymer and extrapolate as that of the grafted polymer brush, actual differences between the free solution polymer and grafted polymer have been reported (e.g., SI-ATRP of methyl methacrylate[58] or styrene[59]).

Robust Surface Mineralization on Ti-pSBMA Substrates. To test the hypothesis that the surface pSBMA polymer brushes grafted from the Ti6Al4V substrate could promote the heterogeneous surface mineralization both in terms of surface mineral coverage and mineral bonding affinity, we subjected Ti-pSBMA-200 substrates and the unmodified Ti6Al4V control to a urea thermal decomposition−mediated mineralization process. This mineralization process was driven by a gradual increase of the pH of an acidic aqueous solution of HA by ammonium hydroxide, generated from controlled thermal decomposition of urea, to induce supersaturation of the mineralization solution and subsequent heterogeneous mineral nucleation and growth.[15,25,45]

Consistent with the findings reported in a previous study on the surface mineralization of unmodified metallic surface (titanium, tantalum, and Ti6Al4V) employing the same mineralization method,[15] a surface coverage of scattered calcium-deficient apatite minerals of 32% was observed on the Ti6Al4V surface (Figure 6a and b). In contrast, much denser spherical mineral nodules composed of platelet-like calcium-deficient apatite crystals (Ca/P ratio: 1.27 ± 0.02) with more than doubled surface coverage (71%) were obtained on the Ti-pSBMA substrates (Figure 6a and b), supporting that the zwitterionic polymer coatings more effectively templated the heterogeneous mineral nucleation and growth. The numerous cationic and anionic residues located along the grafted pSBMA side chains could not only more effectively attract oppositely charged precursor ions than the surface oxides on the unmodified Ti6Al4V but also significantly increase the potential nucleation sites and more effectively reduce the interfacial free energy for heterogeneous nucleation and mineral growth.[25,60]

Equally important, we showed that the surface minerals formed on Ti-pSBMA exhibited more robust adherence to the metallic substrate than those formed on unmodified Ti6Al4V control. Whereas most of the surface minerals on Ti6Al4V could not withstand ultrasonication in water, more than half of the surface minerals formed on the Ti-pSBMA-200 substrate were retained upon identical sonication treatment (Figure 6a and b). Our previous study on the HA-mineralization of 3-D zwitterionic pSBMA hydrogel revealed that the HA mineral growth was directly templated by the zwitterionic ligands, resulting in the detection of the organic zwitterionic ligands within the mineral nodules (supported by high-resolution transmission electron microscopy and associated elemental analysis of the mineral nodules sectioned by focused ion beam).[25] Here, the zwitterionic surface brushes were also likely structurally integrated with the surface minerals as a result of their direct templating role during the surface mineralization, thereby resulting in improved bonding of the surface minerals to the metallic substrate (Figure 6d). We also showed that the extent of surface mineralization including the strongly adhered surface minerals positively correlated with the length of the grafted pSBMA brushes (degree of polymerization, DPs, Figure 6c), further supporting that the surface zwitterionic motifs directly participated in the templated surface-mineralization (Figure 6d).

We also showed that the SI-ATRP of pSBMA and subsequent mineralization could be extended to commercial orthopedic implants with more complex surface topology/porosities. The porous stem region of a Ti6Al4V hip stem (Biomet Taperloc, Complete Hip Stem, Figure 7a and b) was surface grafted with pSBMA (DP = 200) using identical optimized SI-ATRP conditions. Subsequent mineralization showed substantial calcium-deficient apatite mineral (Ca/P = 1.27 ± 0.14) formed throughout the surface of the macropores (yet without blocking the desired macropores) the implant asrevealed by SEM micrographs (Figure 7b) and the associated EDX spectrum (Figure 7c).

Cytocompatibility of the Surface Modifications. Finally, to ensure the cytocompatibility of the surface modifications including the grafting of pSBMA and subsequent surface-mineralization, the viability of bone marrow stromal cells cultured in the presence of pristine Ti6A4 V, Ti-pSBMA, and mineralized Ti-pSBMA (Ti-pSBMA-min) substrates up to 72 h were evaluated and compared with tissue culture
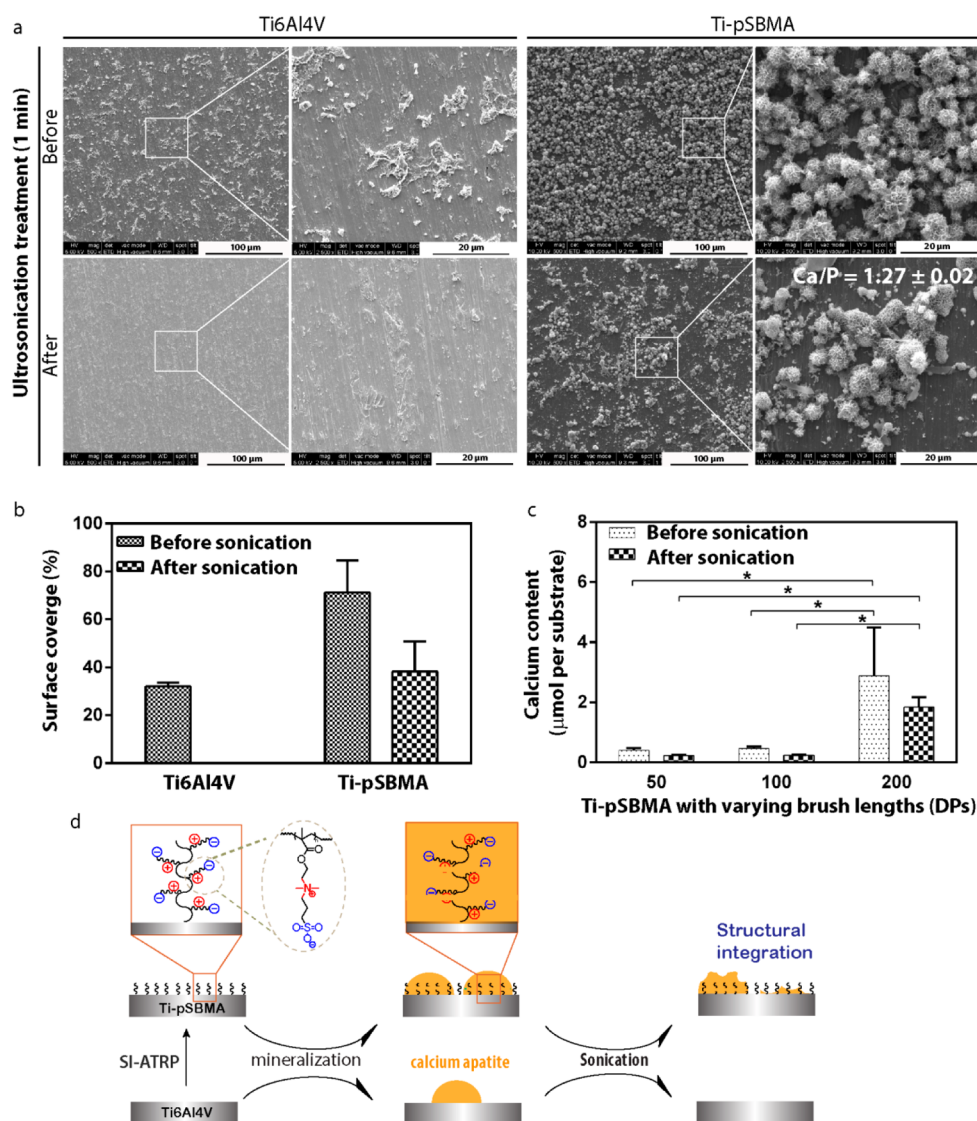
Figure 6. Mineralization on Ti6Al4V substrates with and without surface-grafted pSBMA brushes. (a) SEM micrographs of the mineralized substrates before and after a 1 min ultrasonic treatment. (b) Surface mineral coverage on the substrates as determined by ImageJ ($n = 7$). All differences are significant ($P < 0.05$, two-way ANOVA). (c) Ca^{2+} content on the mineralized Ti-pSBMA substrates ($n = 3$) as a function of degree of polymerization (DPs) of the pSBMA brushes. Differences are not significant ($P > 0.05$, two-way ANOVA) unless denoted as asterisk (*). (d) Schematic illustration of surface mineralization on the pristine Ti6Al4V vs on that surface-grafted with pSBMA brushes.

polystyrene (TCPS) control in the absence of any metal substrates. The cells cultured with the pristine Ti6Al4V substrates were able to proliferate well, resulting in comparable number of viable cells by 72 h compared to those cultured in the absence of any metallic substrates (Figure 8), agreeing with the well-established cytocompatibility of Ti6A4 V.[61] Neither the presence of the zwitterionic pSBMA coating (Ti-pSBMA), known for its biocompatibility, nor the surface mineralization with osteoconductive calcium apatite (Ti-pSBMA-min) compromised the cellular proliferation over 72 h (no significant difference in viable cells compared to those exposed to pristine Ti6Al4V).

■ CONCLUSION

In this study, we reported the preparation of well-controlled zwitterionic pSBMA polymers (PDI < 1.20) through ATRP in an optimized TFE solution containing 10 wt % ionic liquid HMImCl at 60 °C. Equally well-controlled zwitterionic pSBMA

brushes (PDI < 1.20) were fabricated via SI-ATRP from Ti6Al4V substrates covalently tethered with a phosphonic acid based ATRP initiator, conferring biocompatible and antifouling surface properties that are attractive for *in vivo* biomedical applications. The grafted zwitterionic polymer brushes not only effectively templated the surface mineralization, increasing the surface mineral coverage by >100% from those achieved with unmodified Ti6Al4V substrate, but also significantly improved the bonding affinity of the surface apatite minerals to the metallic substrate. The facile surface modification strategy demonstrated here was also extended to real orthopedic implants. The enhanced surface mineralization of metallic implants, combined with its demonstrated cytocompatibility and possible therapeutic delivery of osteoinductive growth factors (e.g., rhBMP-2) via the osteoconductive mineral coating, could potentially improve the osteointegration of the metallic orthopedic and dental implants.
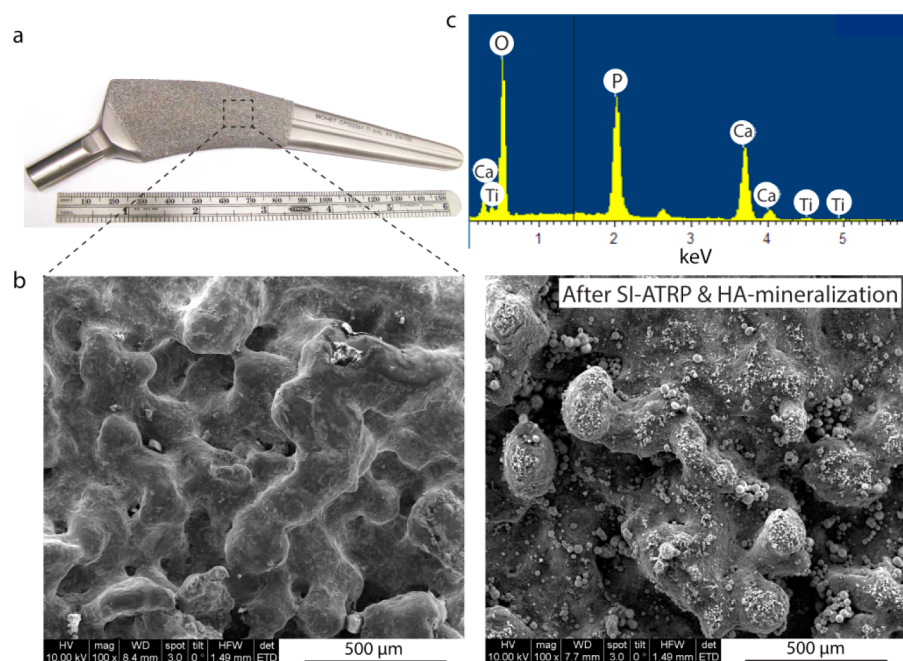
Figure 7. Mineralization on a porous Ti6Al4V hip stem surface-grafted with pSBMA (DP = 200). (a) Photograph of a Taperloc Complete Hip Stem prior to any surface treatment. (b) SEM micrograph of the porous implant surfaces before (left) and after SI-ATRP coating and subsequent mineralization (right). (c) EDX spectrum of the surface calcium apatite minerals.
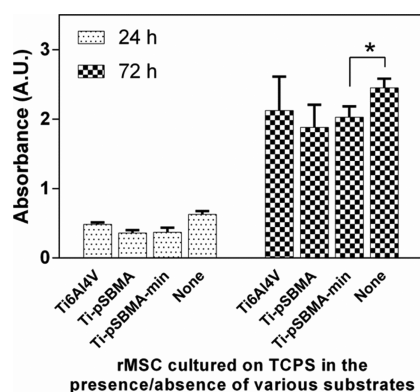
Figure 8. Cell viability of rat MSCs cultured in 24-well culture plate (n = 3) in the presence of Ti6Al4V, Ti-pSBMA, and mineralized Ti-pSBMA substrates. Differences between substrates at a given time point are not significant ($P > 0.05$, two-way ANOVA multiple comparison) unless denoted by an asterisk (*).

■ ASSOCIATED CONTENT

Ⓢ Supporting Information

Synthetic scheme of the phosphonic acid based ATRP initiator (Figure S1), ^{1}H, ^{13}C, and ^{31}P NMR of the initiator (Figures S2−S4), MS spectrum of the initiator (Figure S5), kinetics plots of room temperature solution ATRP without the ionic liquid (Figure S6), GPC curves of the pSBMA polymers obtained from ATRP carried out in TFE/HMImCl at different temperatures (Figure S7). This material is available free of charge via the Internet at http://pubs.acs.org.

■ AUTHOR INFORMATION

Corresponding Author

*Email: jie.song@umassmed.edu.

■ REFERENCES

(1) Long, M.; Rack, H. J. Titanium Alloys in Total Joint Replacement—A Materials Science Perspective. *Biomaterials* **1998**, *19*, 1621−1639.

(2) Hijon, N.; Cabanas, M. V.; Izquierdo-Barba, I.; Vallet-Regi, M. Bioactive Carbonate-Hydroxyapatite Coatings Deposited onto Ti6Al4V Substrate. *Chem. Mater.* **2004**, *16*, 1451−1455.

(3) Hijon, N.; Manzano, M.; Salinas, A. J.; Vallet-Regi, M. Bioactive CaO-SiO$_2$-PDMS Coatings on Ti6Al4V Substrates. *Chem. Mater.* **2005**, *17*, 1591−1596.

(4) Sul, Y. T.; Johansson, C. B.; Petronis, S.; Krozer, A.; Jeong, Y.; Wennerberg, A.; Albrektsson, T. Characteristics of the Surface Oxides on Turned and Electrochemically Oxidized Pure Titanium Implants up to Dielectric Breakdown: the Oxide Thickness, Micropore Configurations, Surface Roughness, Crystal Structure, and Chemical Composition. *Biomaterials* **2002**, *23*, 491−501.

(5) Bandyopadhyay, A.; Espana, F.; Balla, V. K.; Bose, S.; Ohgami, Y.; Davies, N. M. Influence of Porosity on Mechanical Properties and In Vivo Response of Ti6Al4V Implants. *Acta Biomater.* **2010**, *6*, 1640−1648.

(6) Lopez-Heredia, M. A.; Goyenvalle, E.; Aguado, E.; Pilet, P.; Leroux, C.; Dorget, M.; Weiss, P.; Layrolle, P. Bone Growth in Rapid Prototyped Porous Titanium Implants. *J. Biomed. Mater. Res., Part A* **2008**, *85A*, 664−673.

(7) Bose, S.; Roy, M.; Bandyopadhyay, A. Recent Advances in Bone Tissue Engineering Scaffolds. *Trends Biotechnol.* **2012**, *30*, 546−554.

(8) Aparicio, C.; Rodriguez, D.; Gil, F. J. Variation of Roughness and Adhesion Strength of Deposited Apatite Layers on Titanium Dental Implants. *Mater. Sci. Eng., C* **2011**, *31*, 320−324.

(9) Aparicio, C.; Gil, F. J.; Fonseca, C.; Barbosa, M.; Planell, J. A. Corrosion Behaviour of Commercially Pure Titanium Shot Blasted

with Different Materials and Sizes of Shot Particles for Dental Implant Applications. *Biomaterials* **2003**, *24*, 263−273.

(10) Svehla, M.; Morberg, P.; Bruce, W.; Zicat, B.; Walsh, W. R. The Effect of Substrate Roughness and Hydroxyapatite Coating Thickness on Implant Shear Strength. *J. Arthroplasty* **2002**, *17*, 304−311.

(11) Narayanan, R.; Seshadri, S. K.; Kwon, T. Y.; Kim, K. H. Calcium Phosphate-Based Coatings on Titanium and Its Alloys. *J. Biomed. Mater. Res., Part B* **2008**, *85B*, 279−299.

(12) Alghamdi, H. S.; Junker, R.; Bronkhorst, E. M.; Jansen, J. A. Bone Regeneration Related to Calcium Phosphate-Coated Implants in Osteoporotic Animal Models: A Meta-analysis. *Tissue Eng., Part B* **2012**, *18*, 383−395.

(13) Bae, S. E.; Choi, J.; Joung, Y. K.; Park, K.; Han, D. K. Controlled Release of Bone Morphogenetic Protein (BMP)-2 from Nanocomplex Incorporated on Hydroxyapatite-Formed Titanium Surface. *J. Controlled Release* **2012**, *160*, 676−684.

(14) Bose, S.; Tarafder, S. Calcium Phosphate Ceramic Systems in Growth Factor and Drug Delivery for Bone Tissue Engineering: A Review. *Acta Biomater.* **2012**, *8*, 1401−1421.

(15) Liu, P. S.; Smits, J.; Ayers, D. C.; Song, J. Surface Mineralization of Ti6Al4V Substrates with Calcium Apatites for the Retention and Local Delivery of Recombinant Human Bone Morphogenetic Protein-2. *Acta Biomater.* **2011**, *7*, 3488−3495.

(16) Xu, J. W.; Li, X. N.; Lian, J. B.; Ayers, D. C.; Song, J. Sustained and Localized In Vitro Release of BMP-2/7, RANKL, and Tetracycline from FlexBone, an Elastomeric Osteoconductive Bone Substitute. *J. Orthop. Res.* **2009**, *27*, 1306−1311.

(17) Filion, T. M.; Li, X. N.; Mason-Savas, A.; Kreider, J. M.; Goldstein, S. A.; Ayers, D. C.; Song, J. Elastomeric Osteoconductive Synthetic Scaffolds with Acquired Osteoinductivity Expedite the Repair of Critical Femoral Defects in Rats. *Tissue Eng., Part A* **2011**, *17*, 503−511.

(18) Park, J.; Lakes, R. S. *Biomaterials: An introduction.* 3rd ed.; Springer: New York, 2007.

(19) Sun, L. M.; Berndt, C. C.; Gross, K. A.; Kucuk, A. Material Fundamentals and Clinical Performance of Plasma-Sprayed Hydroxyapatite Coatings: A Review. *J. Biomed. Mater. Res.* **2001**, *58*, 570−592.

(20) Kokubo, T.; Takadama, H. How Useful is SBF in Predicting In Vivo Bone Bioactivity? *Biomaterials* **2006**, *27*, 2907−2915.

(21) Traub, W.; Arad, T.; Weiner, S. 3-Dimensional Ordered Distribution of Crystals in Turkey Tendon Collagen Fibers. *Proc. Natl. Acad. Sci. U.S.A.* **1989**, *86*, 9822−9826.

(22) Mann, S. Molecular Recognition in Biomineralization. *Nature* **1988**, *332*, 119−124.

(23) George, A.; Veis, A. Phosphorylated Proteins and Control over Apatite Nucleation, Crystal Growth, and Inhibition. *Chem. Rev.* **2008**, *108*, 4670−4693.

(24) Nudelman, F.; Pieterse, K.; George, A.; Bomans, P. H. H.; Friedrich, H.; Brylka, L. J.; Hilbers, P. A. J.; de With, G.; Sommerdijk, N. A. J. M. The Role of Collagen in Bone Apatite Formation in the Presence of Hydroxyapatite Nucleation Inhibitors. *Nat. Mater.* **2010**, *9*, 1004−1009.

(25) Liu, P.; Song, J. Sulfobetaine as a Zwitterionic Mediator for 3D Hydroxyapatite Mineralization. *Biomaterials* **2013**, *34*, 2442−54.

(26) Banerjee, I.; Pangule, R. C.; Kane, R. S. Antifouling Coatings: Recent Developments in the Design of Surfaces That Prevent Fouling by Proteins, Bacteria, and Marine Organisms. *Adv. Mater.* **2011**, *23*, 690−718.

(27) Chen, S. F.; Li, L. Y.; Zhao, C.; Zheng, J. Surface hydration: Principles and Applications toward Low-Fouling/Nonfouling Biomaterials. *Polymer* **2010**, *51*, 5283−5293.

(28) Ishihara, K.; Nomura, H.; Mihara, T.; Kurita, K.; Iwasaki, Y.; Nakabayashi, N. Why Do Phospholipid Polymers Reduce Protein Adsorption? *J. Biomed. Mater. Res.* **1998**, *39*, 323−330.

(29) Yan, H.; Zhu, H. M.; Shen, J. Molecular Dynamics Simulation Study on Zwitterionic Structure to Maintain the Normal Conformations of Glutathione. *Sci. China, Ser. B: Chem.* **2007**, *50*, 660−664.

(30) Nakaya, T.; Li, Y. J. Phospholipid Polymers. *Prog. Polym. Sci.* **1999**, *24*, 143−181.

(31) Liu, P. S.; Chen, Q.; Wu, S. S.; Shen, J.; Lin, S. C. Surface Modification of Cellulose Membranes with Zwitterionic Polymers for Resistance to Protein Adsorption and Platelet Adhesion. *J. Membr. Sci.* **2010**, *350*, 387−394.

(32) Jiang, S.; Cao, Z. Ultralow-fouling, Functionalizable, and Hydrolyzable Zwitterionic Materials and Their Derivatives for Biological Applications. *Adv. Mater.* **2010**, *22*, 920−952.

(33) Andrew, J. K.; Shaoyi, J. Poly(zwitterionic) Protein Conjugates Offer Increased Stability without Sacrificing Binding Affinity or Bioactivity. *Nat. Chem.* **2012**, *4*, 59−63.

(34) Barbey, R.; Lavanant, L.; Paripovic, D.; Schuwer, N.; Sugnaux, C.; Tugulu, S.; Klok, H. A. Polymer Brushes via Surface-Initiated Controlled Radical Polymerization: Synthesis, Characterization, Properties, and Applications. *Chem. Rev.* **2009**, *109*, 5437−5527.

(35) Wang, W. P.; Cao, H. M.; Zhu, G. J.; Wang, P. A Facile Strategy to Modify TiO$_2$ Nanoparticles via Surface-Initiated ATRP of Styrene. *J. Polym. Sci., Part A: Polym. Chem.* **2010**, *48*, 1782−1790.

(36) Ren, X. S.; Wu, Y. Z.; Cheng, Y.; Ma, H. W.; Wei, S. C. Fibronectin and Bone Morphogenetic Protein-2-Decorated Poly-(OEGMA-r-HEMA) Brushes Promote Osseointegration of Titanium Surfaces. *Langmuir* **2011**, *27*, 12069−12073.

(37) Zhang, F.; Xu, F. J.; Kang, E. T.; Neoh, K. G. Modification of Titanium via Surface-Initiated Atom Transfer Radical Polymerization (ATRP). *Ind. Eng. Chem. Res.* **2006**, *45*, 3067−3073.

(38) Heysel, S.; Vogel, H.; Sanger, M.; Sigrist, H. Covalent Attachment of Functionalized Lipid Bilayers to Planar Wave-Guides for Measuring Protein-Binding to Biomimetic Membranes. *Protein Sci.* **1995**, *4*, 2532−2544.

(39) Xiao, S. J.; Textor, M.; Spencer, N. D.; Wieland, M.; Keller, B.; Sigrist, H. Immobilization of the Cell-Adhesive Peptide Arg-Gly-Asp-Cys (RGDC) on Titanium Surfaces by Covalent Chemical Attachment. *J. Mater. Sci.:Mater. Med.* **1997**, *8*, 867−872.

(40) Xiao, S. J.; Textor, M.; Spencer, N. D.; Sigrist, H. Covalent Attachment of Cell-Adhesive, (Arg-Gly-Asp)-Containing Peptides to Titanium Surfaces. *Langmuir* **1998**, *14*, 5507−5516.

(41) Rezania, A.; Johnson, R.; Lefkow, A. R.; Healy, K. E. Bioactivation of Metal Oxide Surfaces. 1. Surface Characterization and Cell Response. *Langmuir* **1999**, *15*, 6931−6939.

(42) Marcinko, S.; Fadeev, A. Y. Hydrolytic Stability of Organic Monolayers Supported on TiO$_2$ and ZrO$_2$. *Langmuir* **2004**, *20*, 2270−2273.

(43) Lafond, V.; Gervais, C.; Maquet, J.; Prochnow, D.; Babonneau, F.; Mutin, P. H. O-17 MAS NMR Study of the Bonding Mode of Phosphonate Coupling Molecules in a Titanium Oxo-alkoxo-phosphonate and in Titania-Based Hybrid Materials. *Chem. Mater.* **2003**, *15*, 4098−4103.

(44) Terayama, Y.; Kikuchi, M.; Kobayashi, M.; Takahara, A. Well-Defined Poly(sulfobetaine) Brushes Prepared by Surface-Initiated ATRP Using a Fluoroalcohol and Ionic Liquids as the Solvents. *Macromolecules* **2011**, *44*, 104−111.

(45) Song, J.; Saiz, E.; Bertozzi, C. R. A New Approach to Mineralization of Biocompatible Hydrogel Scaffolds: An Efficient Process toward 3-Dimensional Bonelike Composites. *J. Am. Chem. Soc.* **2003**, *125*, 1236−1243.

(46) Tas, A. C. Molten Salt Synthesis of Calcium Hydroxyapatite Whiskers. *J. Am. Ceram. Soc.* **2001**, *84*, 295−300.

(47) Lee, W. F.; Chen, C. F. Poly(2-hydroxyethyl methacrylate-co-sulfobetaine)s Hydrogels: 3. Synthesis and Swelling Behaviors of the [2-Hydroxyethyl methacrylate-co-N,N′-dimethyl (acrylamido propyl) ammonium propane sulfonate] Hydrogels. *Polym. Gels Networks* **1998**, *6*, 493−511.

(48) Jiang, S.; Gao, C. L.; Li, G. Z.; Xue, H.; Brault, N. D. Zwitterionic Polymers Having Biomimetic Adhesive Linkages. U.S. Patent 2011/0105712, May 5, 2011.

(49) Kobayashi, M.; Terada, M.; Terayama, Y.; Kikuchi, M.; Takahara, A. Direct Synthesis of Well-Defined Poly{2-(methacryloyloxy)ethyl}trimethylammonium Chloride Brush via Sur-

7151

dx.doi.org/10.1021/am501967y | *ACS Appl. Mater. Interfaces* 2014, 6, 7141−7152

face-Initiated Atom Transfer Radical Polymerization in Fluoroalcohol. *Macromolecules* **2010**, *43*, 8409−8415.

(50) Wasserman, S. R.; Whitesides, G. M.; Tidswell, I. M.; Ocko, B. M.; Pershan, P. S.; Axe, J. D. The Structure of Self-Assembled Monolayers of Alkylsiloxanes on Silicon—A Comparison of Results from Ellipsometry and Low-Angle X-ray Reflectivity. *J. Am. Chem. Soc.* **1989**, *111*, 5852−5861.

(51) Zhang, Z.; Chao, T.; Chen, S. F.; Jiang, S. Y. Superlow Fouling Sulfobetaine and Carboxybetaine Polymers on Glass Slides. *Langmuir* **2006**, *22*, 10072−10077.

(52) Yuan, Y. L.; Zhang, J.; Ai, F.; Yuan, J.; Zhou, J.; Shen, J.; Lin, S. C. Surface Modification of SPEU Films by Ozone Induced Graft Copolymerization to Improve Hemocompatibility. *Colloids Surf., B* **2003**, *29*, 247−256.

(53) Chang, Y.; Chen, S. F.; Zhang, Z.; Jiang, S. Y. Highly Protein-Resistant Coatings from Well-Defined Diblock Copolymers Containing Sulfobetaines. *Langmuir* **2006**, *22*, 2222−2226.

(54) Liu, P. S.; Chen, Q.; Liu, X.; Yuan, B.; Wu, S. S.; Shen, J.; Lin, S. C. Grafting of Zwitterion from Cellulose Membranes via ATRP for Improving Blood Compatibility. *Biomacromolecules* **2009**, *10*, 2809−2816.

(55) Smith, R. S.; Zhang, Z.; Bouchard, M.; Li, J.; Lapp, H. S.; Brotske, G. R.; Lucchino, D. L.; Weaver, D.; Roth, L. A.; Coury, A.; Biggerstaff, J.; Sukavaneshvar, S.; Langer, R.; Loose, C. Vascular Catheters with a Nonleaching Poly-sulfobetaine Surface Modification Reduce Thrombus Formation and Microbial Attachment. *Sci. Transl. Med.* **2012**, *4*, 1−10.

(56) Wang, J. S.; Matyjaszewski, K. Controlled Living Radical Polymerization—Atom-Transfer Radical Polymerization in the Presence of Transition Metal Complexes. *J. Am. Chem. Soc.* **1995**, *117*, 5614−5615.

(57) Matyjaszewski, K.; Xia, J. H. Atom Transfer Radical Polymerization. *Chem. Rev.* **2001**, *101*, 2921−2990.

(58) Marutani, E.; Yamamoto, S.; Ninjbadgar, T.; Tsujii, Y.; Fukuda, T.; Takano, M. Surface-Initiated Atom Transfer Radical Polymerization of Methyl Methacrylate on Magnetite Nanoparticles. *Polymer* **2004**, *45*, 2231−2235.

(59) Koylu, D.; Carter, K. R. Stimuli-Responsive Surfaces Utilizing Cleavable Polymer Brush Layers. *Macromolecules* **2009**, *42*, 8655−8660.

(60) Mann, S. *Biomineralization: Principles and Concepts in Bioinorganic Materials Chemistry*; Oxford University Press: Oxford, 2001.

(61) Bruni, S.; Martinesi, M.; Stio, M.; Treves, C.; Bacci, T.; Borgioli, F. Effects of Surface Treatment of Ti-6Al-4V Titanium Alloy on Biocompatibility in Cultured Human Umbilical Vein Endothelial Cells. *Acta Biomater.* **2005**, *1*, 223−234.